

pubs.acs.org/JPCA Article

Coulomb Explosion Dynamics of Multiply Charged *para*-Nitrotoluene Cations

Jacob M. Shusterman, Gennady L. Gutsev, Hugo A. López Peña, B. Ramu Ramachandran, and Katharine Moore Tibbetts*



Cite This: J. Phys. Chem. A 2022, 126, 6617–6627



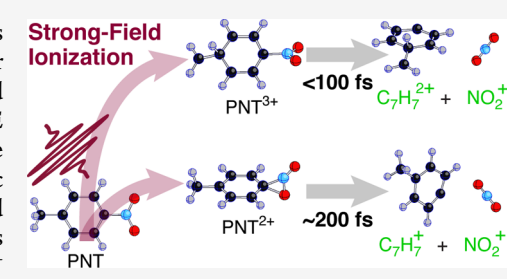
ACCESS

III Metrics & More

Article Recommendations

s Supporting Information

ABSTRACT: This work explores Coulomb explosion (CE) dissociation pathways in multiply charged cations of *para*-nitrotoluene (PNT), a model compound for nitroaromatic energetic molecules. Experiments using strong-field ionization and mass spectrometry indicate that metastable cations PNT²⁺ and PNT³⁺ undergo CE to produce NO₂⁺ and NO⁺. The experimentally measured kinetic energy release from CE upon formation of NO₂⁺ and NO⁺ agrees qualitatively with the kinetic energy release predicted by computations of the reaction pathways in PNT²⁺ and PNT³⁺ using density functional theory (DFT). Both DFT computations and mass spectrometry identified additional products from CE of highly charged PNT^{q+} cations with q > 3. The dynamical timescales required for direct CE of PNT²⁺ and



PNT³⁺ to produce NO₂⁺ were estimated to be 200 and 90 fs, respectively, using ultrafast disruptive probing measurements.

1. INTRODUCTION

Electronic excitation, ionization, and electron-ion coupling play crucial roles in shock initiation of energetic materials. ^{1–3} In particular, ionization of the parent energetic molecules lowers the barrier to molecular dissociation in explosives including TNT, RDX, and PETN, thereby facilitating the initiation of detonation. ^{4,5} Moreover, laser initiation of photoactive explosives produces electronic excited states and ions to selectively initiate detonation. ^{6–8} Hence, knowledge of the initial dissociation pathways of ionized energetic molecules is important for advancing the understanding of initiation mechanisms in energetic materials and designing safer photoactive explosives.

Strong-field ionization (SFI) with intense femtosecond laser pulses coupled to mass spectrometry has been used for decades to study unimolecular dissociation pathways in ionized nitroorganic energetic molecules. 9-12 The extremely high intensities produced by SFI have enabled detection of fragmentation products produced from both singly- and multiply-charged cations in the explosive TNT¹³ and model systems including nitrobenzenes, nitrotoluenes, and nitromethane. 12-15 In particular, Coulomb explosion (CE) of multiply charged precursor ions has been identified in the NO2 and NO+ signals from these nitro-organic molecules upon SFI, on the basis of the characteristic splitting of peaks in the mass spectrum around the nominal m/z value. 13-15 The kinetic energy released by CE to produce NO+ and NO2+ has been measured for multiple nitroaromatic molecules, 13 and the computed energetics of nitromethane dication dissociation to produce CH₃⁺ and NO₂⁺ were found to match the experimental kinetic energy release. 15 However, both the CE reaction pathways and their dynamical timescales in nitroaromatic molecules have yet to be elucidated.

Time-resolved "pump—probe" measurements using an intense pump to induce SFI, followed by a weak probe pulse to electronically excite cations, also called "ultrafast disruptive probing", 16 can identify timescales involved in dissociation pathways of singly- and multiply-charged cations. Using this technique, our group recently found that nitro-nitrite rearrangement in the nitromethane cation with subsequent NO+ loss occurs in $\sim\!440~{\rm fs}^{17}$ and identified coherent vibrational motions in nitrobenzene and nitrotoluene cations with $\sim\!400~{\rm fs}$ period, that facilitates direct C–N bond cleavage. $^{18-21}$ Others have used ultrafast disruptive probing to determine timescales required for ${\rm H_3^+}$ formation from dications of small alcohols $^{22-24}$ and pump—probe measurements with extreme-ultraviolet pump pulses to determine CE timescales in methanol, $^{25}~{\rm N}_2{\rm O}$, $^{26}~{\rm and}~{\rm CO}_2$.

In this work, we use SFI and ultrafast disruptive probing with complementary quantum chemical calculations to determine CE reaction pathways and dynamical timescales for dissociation of multiply charged cations of *para*-nitrotoluene (PNT), a model compound for the explosive TNT. Analysis of the CE ion signals of NO₂⁺ and NO⁺ indicate that SFI under our experimental conditions produces both PNT

Received: June 24, 2022 Revised: August 29, 2022 Published: September 20, 2022





dication (PNT²⁺) and trication (PNT³⁺) that undergo rapid CE. The experimental kinetic energy released from CE of PNT²⁺ and PNT³⁺ agrees qualitatively with the reaction pathways computed by DFT. Ultrafast disruptive probing measurements indicate that direct CE to produce NO₂⁺ occurs in approximately 200 fs for PNT²⁺ and 90 fs for PNT³⁺.

2. METHODS

2.1. Experiment. The full experimental setup has been described in detail in our previous work.²¹ Briefly, a commercial Ti:sapphire regenerative amplifier (Astrella, Coherent, Inc.) producing 30 fs, 800 nm, 2.2 mJ pulses is used to pump an optical parametric amplifier (OPA, TOPAS Prime) to produce 20 fs, 1300 nm pump pulses. 1300 nm was selected as the pump wavelength because wavelengths in the 1200-1600 nm range are widely observed to decrease molecular dissociation, relative to 800 nm due to an enhanced contribution of adiabatic tunneling ionization, relative to nonadiabatic multiphoton ionization. To achieve a 400 nm probe pulse, a portion of the 800 nm output beam that was split with a 90:10 (r:t) beam splitter before the OPA was frequency-doubled with a BBO crystal. Pump energy attenuation from 60 to 5 μ J was accomplished by adjusting an achromatic half-wave plate placed before a polarizing cube, resulting in peak laser intensities in the range of 2×10^{13} W cm⁻² to 2×10^{14} W cm⁻². The probe intensity was selected to be $6 \times 10^{12} \text{ W cm}^{-2}$, sufficient to electronically excite ionized species but too low to create ions on its own. Pump and probe beams were focused into the extraction region of a linear timeof-flight (TOF) mass spectrometer with an f = 20 cm fused silica lens. The linear polarization of the laser electric field was parallel to the ion TOF axis. The 400 nm probe pulse duration was estimated as 70.5 fs from the fwhm of the cross-correlation of the O2 signal from air in the mass spectrometer with 1300 nm pump/400 nm probe excitation, keeping in mind that the fwhm is determined by the longer of the two pulses and is directly related with the temporal resolution of the experiment.²¹ PNT (99%, Sigma-Aldrich) was introduced into a vacuum chamber via an effusive inlet with gentle heating. Mass spectra were recorded and averaged with a 1 GHz digital oscilloscope (LeCroy WaveRunner 610Zi). Under these conditions, the 2 ns resolution of the TOF acquisition resulted in a resolution of $\sim 0.4-1.6$ eV in the kinetic energy release we can measure, depending on the fragment (c.f., Section 3.2).

2.2. Theory. Our computations were performed by using density functional theory (DFT) with a hybrid long-range corrected exchange–correlation functional ω B97X-D with damped atom–atom dispersion corrections, ³² which was found to provide the best agreement with the experiment among several other methods for *ortho*-nitrotoluene. ¹⁹ The augmented correlation-consistent Dunning's basis set aug-cc-pVTZ³³ was chosen to be consistent with our previous work on multiply charged nitromethane cations. ¹⁵ The adiabatic ionization energy computed for PNT at the ω B97X-D/aug-cc-pVTZ level is 9.32 eV and compares quite well with the accepted experimental value of 9.46 \pm 0.05 eV. ³⁴

Extensive search was performed for isomers of PNT^{q^+} up to q = 8. Each geometry optimization was followed by harmonic frequency computations to confirm that the state with this geometry corresponds to a local minimum on the potential energy surface. It was found that metastable isomers do exist up to q = 7 (Supporting Information, Figures S1–S6). However, when optimization starts with the geometry of

neutral ground-state PNT, the charge states with $q \ge 4+$ are unstable (vide infra). The lowest energy isomers of both PNT⁺ and PNT²⁺ are formed by moving a hydrogen atom from the CH₃ moiety to oxygen of the NO₂ group to form NOOH, and the lowest-energy PNT³⁺ isomer has a nearly planar zigzagtype shape. The states of PNT⁺, PNT²⁺, and PNT³⁺ with the neutral PNT topology are higher by +0.77, +2.45, and +3.38 eV, respectively, than the lowest energy isomers for each charge state.

To check the robustness of the results obtained for the charged states, we performed computations of the vertical ionization energies of PNT using the Pople's $6-311+G^*$ and 6-311+G(3df) basis sets.³⁵ As can be seen from Table 1, the

Table 1. Computed Vertical Ionization Energies in eV of PNT Cations Using ω B97X-D

initial PNT^{q+}	final PNT^{q+}	6-311+G*	6-311+G(3df)	aug-cc-PVTZ
0	1	9.71	9.65	9.63
1	0	15.17	15.12	15.08
1	2	15.42	15.37	15.34
2	3	20.31	20.28	20.26
3	2	26.00	25.98	25.95
3	4	25.40	25.38	25.36
4	5	30.40	30.47	30.40

results obtained using three different basis sets and the ω B97X-D functional agree to within 0.1 eV. The adiabatic ionization energies (Supporting Information, Table S1) show a similar dependence on the basis set. Although the adiabatic ionization energies computed with Pople's basis sets compare slightly better with experiments, we prefer to use the more flexible augcc-PVTZ basis.

The energies and oscillator strengths for transitions to electronic excited states in PNT cations were performed by using time-dependent DFT (TDDFT)³⁶ and equation of motion coupled cluster with single and double excitations (EOM-CCSD),³⁷ as realized in Gaussian 16.³⁸ The TDDFT calculations used the ω B97X-D functional with the aug-cc-PVTZ basis, while the non-augmented cc-PVTZ basis was used in our EOM-CCSD calculations.

To explore stability of PNT²⁺ and PNT³⁺ toward the loss of NO⁺ and NO⁺, we performed the search for the corresponding dissociation pathways from initial to final states. The modified conjugate gradient algorithm developed by Schlegel³⁹ was used for search of transition states (TSs) possessing a single imaginary frequency. The intrinsic reaction coordinate (IRC) method, connecting a TS to initial and product states, ^{40,41} was used to find dissociation pathways. Charges on atoms were determined from the NBO analysis. ⁴²

3. RESULTS AND DISCUSSION

3.1. Multiple Ionization of PNT. Figure 1 shows the vertical and adiabatic ionization energies for PNT to produce cation states up to PNT³⁺. The intact PNT⁺ cation has been observed in multiple SFI mass spectrometry investigations, 10,14,18,20,21 and according to our previous calculations, PNT⁺ is stable to NO₂ loss by 1.89 eV at the B3LYP/Def2TZVPP level. According to our present computations at the ω B97X-D/aug-cc-PVTZ level, the cation states PNT²⁺ and PNT³⁺ are metastable with respect to NO₂ loss by at least 0.2 eV (Supporting Information, Figure S7), so the adiabatic ionization energy for each state is well defined. For all three

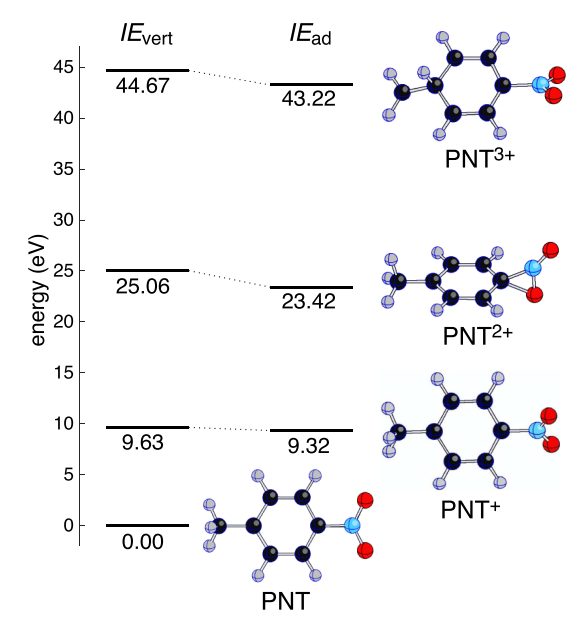


Figure 1. Vertical and adiabatic ionization energies of PNT, computed at the ω B97X-D/aug-cc-PVTZ level.

cation charge states, the NO_2 group rotates out-of-plane with respect to the benzene ring. Moreover, the large adiabatic corrections to the ionization energies for both the dication and trication can be attributed to their additional geometry changes with respect to those of the neutral PNT: the NO_2 group in PNT²⁺ exhibits C–O bonding, and an H atom from the methyl group migrates to the benzene ring in PNT³⁺. Although the tetracation PNT⁴⁺ with the neutral topology is geometrically stable at the ω B97X-D/aug-cc-PVTZ level (Supporting Information, Figure S5), it is metastable to NO_2 loss by only 0.05 eV (Supporting Information, Figure S7), so it is not included in Figure 1.

Figure 2 shows the decay products obtained from highly charged PNT $^{q+}$ cations with q=5-10 upon optimization of the polycations, starting with the neutral PNT ground state geometry. Numerous small charged fragments including O^+ , CH^+ , C^+ , and H^+ are formed from various initial charge states. The benzene ring remains partially intact (excepting hydrogen losses) for charge states up to q=+9e but completely fragments at q=+10e.

To assess the stability of PNT^{q+} cations and identify CE products experimentally, SFI mass spectra were recorded using 1300 nm, 20 fs pulses at intensities ranging from 2×10^{13} to 2 \times 10¹⁴ W cm⁻². Figure 3 displays the mass spectra of PNT recorded at 8×10^{13} W cm⁻² (blue, top) and 2×10^{14} W cm⁻² (red, bottom). At both intensities, the parent PNT+ ion is more than twice as intense as the C₇H₇⁺ fragment, which confirms that SFI at 1300 nm induces less nonadiabatic dissociation of PNT+ than that found in earlier studies using SFI at 800 nm.11-14 The enhanced yield of intact PNT+ is consistent with the increasing contribution of adiabatic electron tunneling ionization, which results in enhanced population of cations in their electronic ground state. 18,28-31 Nevertheless, no intact PNT^{q+} ions with $q \ge 2$ are observed. Instead, substantial fragmentation due to CE is observed, particularly at high intensity, where NO₂⁺, NO⁺, C⁺, and H⁺ are produced in high yields.

The inset panels (a-f) in Figure 3 magnify specific m/z regions of ions produced by CE, which have split peak

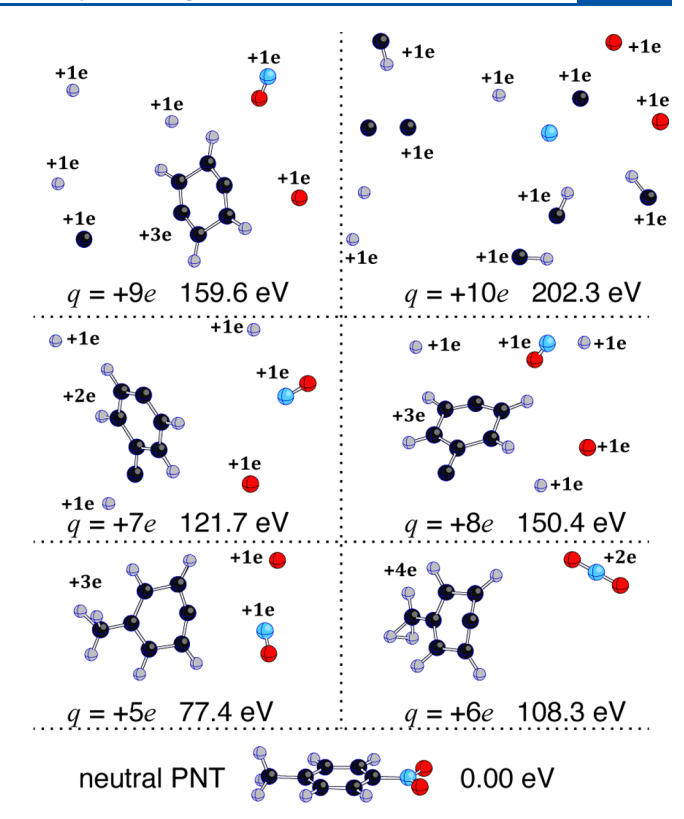


Figure 2. Decay products of highly charged PNT $^{q+}$ cations (q = 5-10) obtained upon optimizations beginning with the neutral ground state geometry at the ω B97X-D/aug-cc-PVTZ level. The spin multiplicity was 2S + 1 = 1 and 2 for the systems with even and odd numbers of electrons, respectively.

structures at each m/z value corresponding to fragments ejected toward and away from the detector. At a moderate laser intensity of $8 \times 10^{13} \text{ W cm}^{-2}$, CE is evident in both the $C_7H_n^+$ (m/z 84-91, Figure 3c) and $C_7H_n^{2+}$ (m/z 42.5-45.5, Figure 3b). The peak at m/z 43 is assigned to $C_7H_2^{2+}$ on the basis of the identification of this species and other $C_7H_n^{2+}$ from X-ray photoionization of toluene⁴³ and in a previous SFI study of meta-nitrotoluene. 12 The higher laser intensity of 2×10^{14} W cm $^{-2}$ results in numerous $C_2H_{\it n}^{\scriptscriptstyle +}$ and $CH_{\it n}^{\scriptscriptstyle +}$ fragmentation products with either well-defined split-peak structures or substantial peak broadening indicative of CE (Figure 3e,f), along with multiply charged atoms C³⁺, O³⁺, C²⁺, N²⁺, and O²⁺ (Figure 3d). These fragments and multiply charged atoms have also been observed with SFI at 800 nm, 12 albeit at an order of magnitude higher laser intensity than that used in our experiments. The higher laser intensities required to observe multiply charged atoms using 800 nm SFI arise because the transition from multiphoton ionization to tunneling ionization occurs at substantially higher intensity at 800 nm. 28 We also observe the multiply charged molecules C₄H₃²⁺ (Figure 3f) and potentially $C_4H_3^{3+}$ (Figure 3e), although we cannot rule out contributions from OH^+ to the m/z 17 peak assigned to $C_4H_3^{3+}$. Nevertheless, calculations at the ω B97X-D/aug-cc-PVTZ level (Supporting Information, Figure S8) indicate that $C_4H_3^{q+}$ is geometrically stable up to q=4.

Unlike the hydrocarbon fragments and atoms that exhibit a single pair of CE peaks, both the NO⁺ (Figure 3a) and NO₂⁺ (Figure 3b) fragments exhibit two distinct pairs of CE peaks labeled by the red and green circles, respectively. Previous studies of PNT and related nitroaromatics using 800 nm SFI

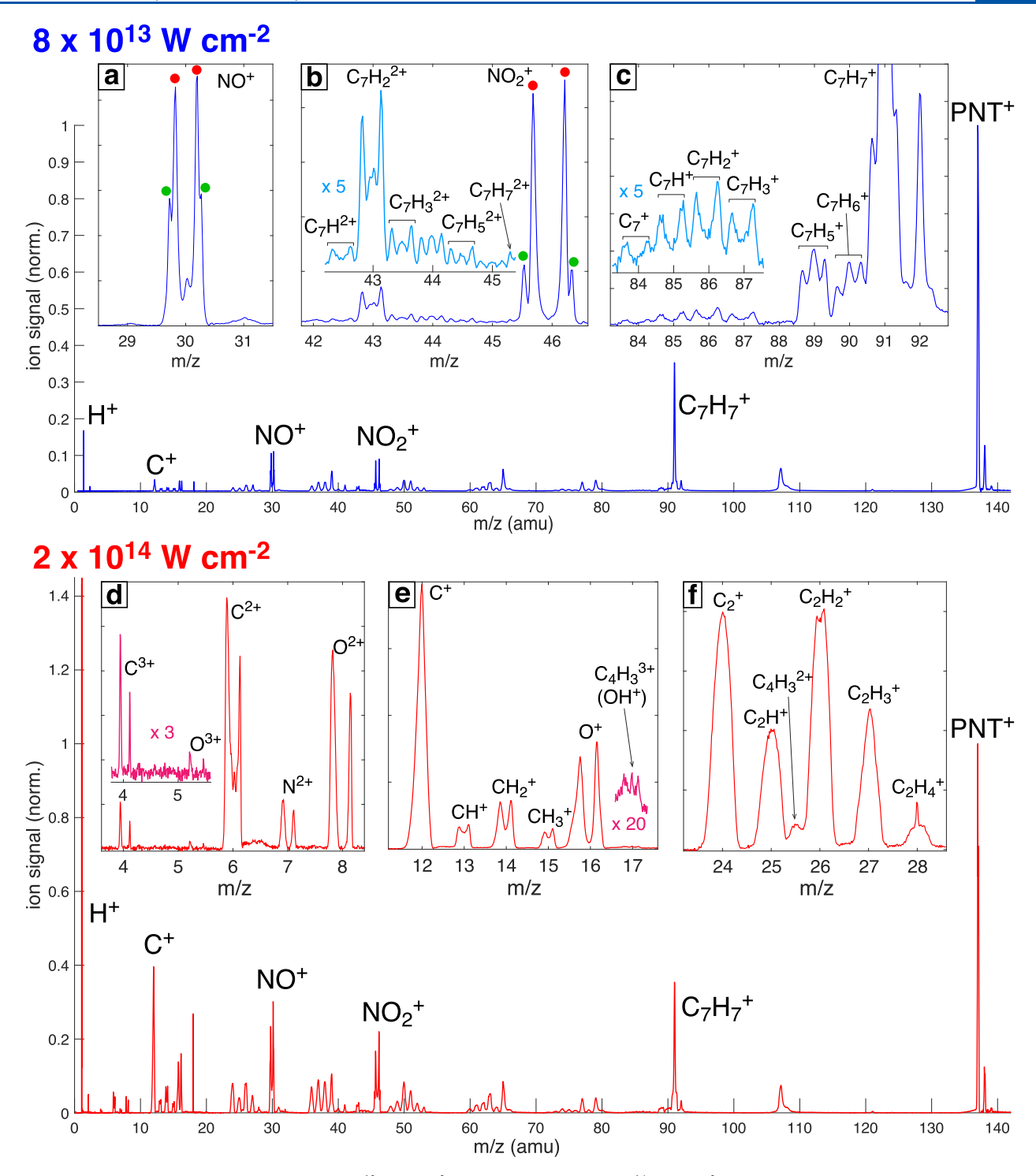


Figure 3. SFI mass spectrum of PNT at $8 \times 10^{13} \text{ W cm}^{-2}$ (blue, top) and $2 \times 10^{14} \text{ W cm}^{-2}$ (red, bottom) with insets showing selected fragmentation products produced by CE: NO⁺ (a); NO⁺₂ and $C_7H_n^{2+}(b)$; $C_7H_n^{+}(c)$; multiply charged atomic ions (d); CH⁺_n(e); and C₂H⁺_n(f). Red and green circles in panels (a,b) denote CE peaks assigned to different precursor charge states, as explained in the text.

only observed a single pair of CE peaks in NO_2^+ and NO^+ signals. ^{13,14} The presence of two pairs of CE peaks in a specific ion signal indicates that the ion can be formed by two distinct CE pathways that release different kinetic energies (KEs). Previous investigations of CE in N_2^{44} and CH_3^{45} have assigned the separate pairs of peaks to different initial charge states of the precursor ion, where the peaks associated with higher KE release were assigned to a higher initial charge state. Considering a PNT cation with initial charge q+ undergoing

cleavage of the C–N bond through CE, the pathways can be written as $PNT^{q+} \rightarrow NO_2^+ + C_7H_7^{(q-1)+}$. On this basis, we assign the low-KE peaks (red) to q=2 and the high-KE peaks (green) to q=3 for both the NO^+ and NO_2^+ signals.

To confirm these charge state assignments, the intensity dependence of the CE yields of NO⁺ and NO⁺₂, along with the hydrocarbon fragments $C_7H_2^{2+}$ and $C_7H_7^{+}$ are plotted in Figure 4. The yields of intact PNT⁺ and the central peak of $C_7H_7^{+}$ (i.e., originating from a singly charged precursor) are plotted for

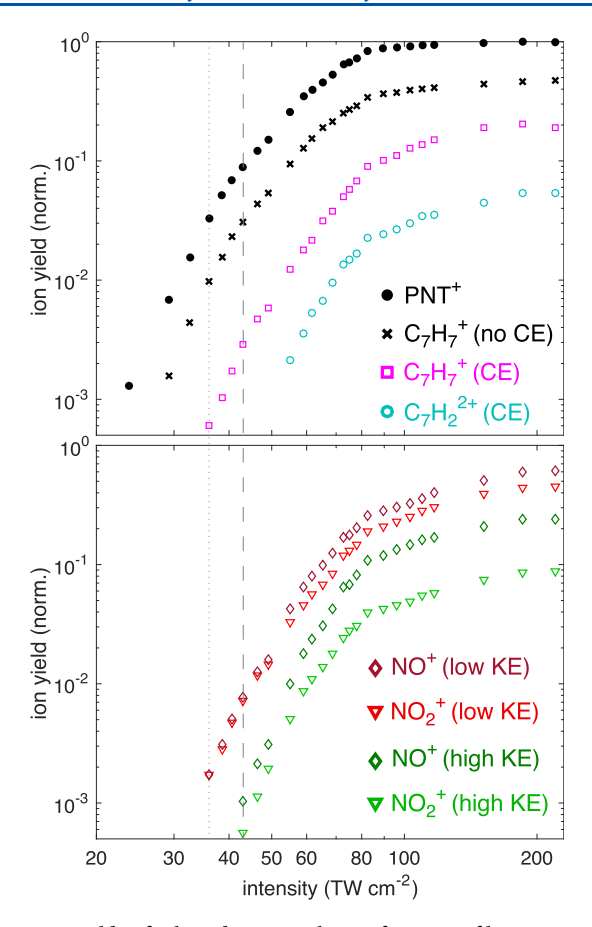


Figure 4. Yields of selected ion signals as a function of laser intensity. Proposed intensity thresholds for formation of PNT²⁺ and PNT³⁺, indicated by dotted and dashed lines.

comparison. To resolve the two pairs of CE peaks in NO⁺ and NO₂, along with the CE and non-CE contributions to C₇H₇⁺ and $C_7H_2^{2+}$, the ion signals were fit to a series of Gaussian functions using literature methods.^{44,45} Examples of fitting results for each ion shown in Figure 4 are provided in the Supporting Information, Figure S9. In Figure 4, PNT+ and non-CE C₇H₇⁺ (black symbols) appear at intensities below 30 TW cm⁻², where only singly charged PNT⁺ is formed. At 35 TW cm⁻² (vertical dotted line), both low-KE signals for NO⁺ and NO₂ and CE signals from C₇H₇ appear. The high-KE signals for NO⁺ and NO⁺ first appear at a higher intensity of 42 TW cm⁻² (vertical dashed line). These distinct threshold intensities support the assignment of the low-KE CE peaks to precursor PNT²⁺ and the high-KE CE peaks to PNT³⁺. C₇H₂²⁺ first appears at a higher intensity of 55 TW cm⁻², which indicates that it requires an initial charge state of at least PNT³⁺, although we cannot rule out the possibility that its formation requires an initial charge state of PNT⁴⁺ or higher.

3.2. CE Pathways of PNT²⁺ **and PNT**³⁺. Having assigned the pairs of low-KE and high-KE CE peaks in the NO⁺ and NO⁺₂ ion signals to initial PNT^{q+} charge states with q = 2 and q = 3, respectively, we consider two possible dissociation pathways from each initial precursor: a "direct" pathway producing NO⁺₂ (eqs 1 and 2) and a "rearrangement" pathway producing NO⁺ (eqs 3 and 4)

$$PNT^{2+} \to NO_2^+ + C_7H_7^+$$
 (1)

$$PNT^{3+} \to NO_2^+ + C_7 H_7^{2+}$$
 (2)

$$PNT^{2+} \rightarrow NO^{+} + C_{7}H_{7}O^{+} \tag{3}$$

$$PNT^{3+} \to NO^{+} + C_7 H_7 O^{2+}$$
 (4)

Computation of these pathways shows that both the direct and rearrangement pathways for PNT²⁺ and PNT³⁺ occur through single TSs (Figure 5). The small barriers to dissociation are

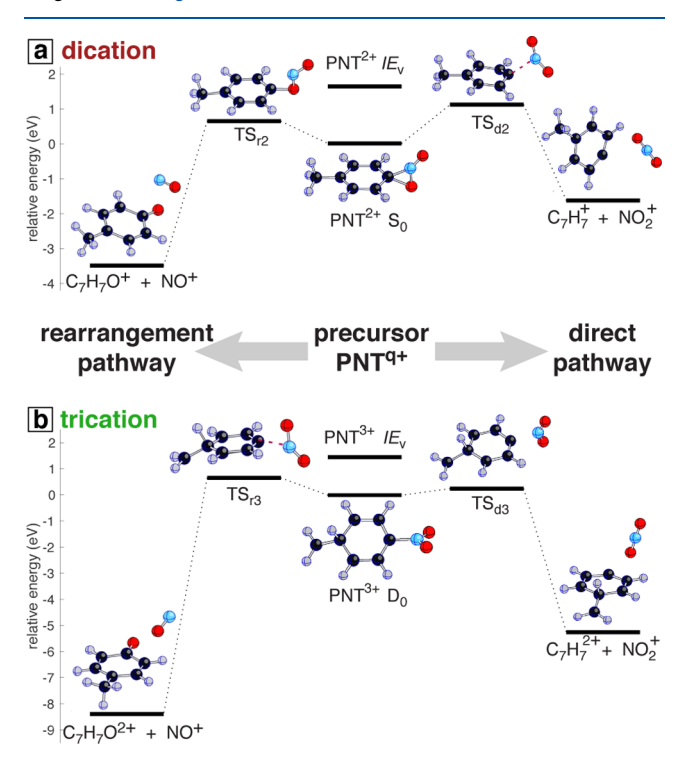


Figure 5. Pathways to the loss of NO $^+$ ("rearrangement", left) and NO $_2^+$ ("direct", right) from PNT $^{2+}$ (a, top) and PNT $^{3+}$ (b, bottom), computed at the ω B97X-D/aug-cc-PVTZ level. The vertical ionization energies (indicated as IE $_v$) exceed each TS energy, making all pathways spontaneous.

inside the range between 0.24 and 1.12 eV. Therefore, the excess energy imparted from vertical ionization to PNT²⁺ or PNT³⁺ makes both direct and rearrangement pathways spontaneous, which accounts for the lack of intact multiply charged PNT cations seen in the mass spectra. We note that only $C_7H_7^+$ from the pathway in eq 1 is definitively observed as CE peaks in the mass spectra (Figure 3c), although a small amount of $C_7H_7^{2+}$ appears to be present at m/z 45.5 but mostly obscured by the adjacent NO_2^+ signal (Figure 3b). No direct evidence of $C_7H_7O^+$ or $C_7H_7O^{2+}$ was found in the mass spectra, which suggests that these species further dissociate into smaller fragments.

The computational results shown in Figure 5 indicate that direct CE upon vertical ionization should release 3.26 eV of KE for PNT²⁺ and 6.72 eV for PNT³⁺. Similarly, the rearrangement pathways should release 5.12 eV for PNT²⁺ and 9.85 eV for PNT³⁺. For comparison to these calculated values of energy release, we can evaluate the experimental KE distributions of ion signals obtained from CE by transforming the flight time axis into the kinetic energy via the formula⁴⁴

$$E_{k} = \frac{(zeF)^{2}}{2m}(t - t_{0})^{2} \tag{5}$$

where z is the charge of the fragment, e is the elementary charge, F is the electric field strength between the ion repeller and extraction plates, m is the mass of the fragment, t is the flight time, and t_0 is the flight time corresponding to zero kinetic energy release.

Figure 6 shows the KE distributions obtained from the CE ion signals of NO^+ , NO_2^+ , $C_7H_7^+$, and $C_7H_2^{2+}$. Fitting these

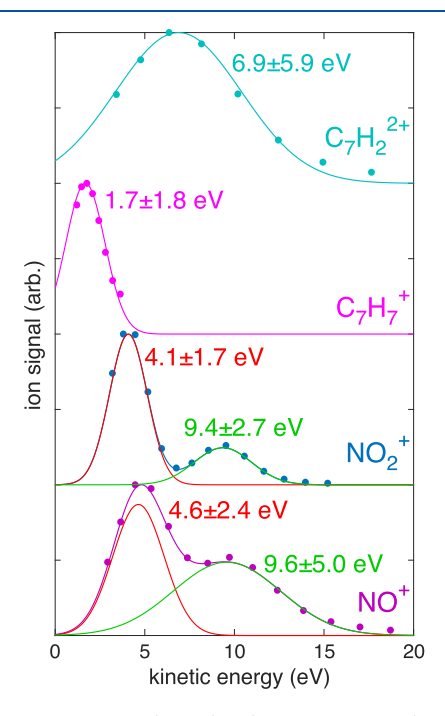


Figure 6. Kinetic energy release distributions computed via eq 5 from NO $^+$, NO $^+$, $C_7H_7^+$, and $C_7H_2^{2+}$ ion signals (dots) with Gaussian fits (solid lines). The indicated KE release values denote the mean and fwhm of each Gaussian fit component.

distributions to one (for $C_7H_7^+$ and $C_7H_2^{2+}$) or two (for NO^+ and NO₂⁺) Gaussian functions yielded the mean KE release and fwhm values indicated on the plot. The NO₂⁺ ion signals explode with somewhat higher KE release than that computed for direct CE in both PNT²⁺ (4.1 \pm 1.7 eV vs 3.26 eV) and PNT^{3+} (9.4 \pm 2.7 eV vs 6.72 eV). In contrast, the KE release from the NO+ ion signals is slightly lower than the computed values for rearrangement of CE for both PNT²⁺ (4.6 \pm 2.4 eV vs 5.12 eV) and PNT³⁺ (9.6 \pm 5.0 eV vs 9.85 eV), although both calculated values are within the experimental uncertainty. For comparison, $C_7H_7^+$ explodes with 1.7 \pm 1.8 eV and $C_7H_7^{2+}$ explodes with 6.9 \pm 5.9 eV. $C_7H_7^+$ is attributed to direct CE via eq 1, which brings the total estimated KE release from this pathway to ~ 5.8 eV. Although $C_7H_2^{2+}$ cannot definitively be assigned to CE of PNT³⁺, as discussed earlier, if this signal is a secondary product from eqs 2 and/or 4, it would bring the total KE release from both CE pathways of PNT³⁺ to ~16 eV.

3.3. Dynamical Timescales of Direct CE Pathways. Ultrafast disruptive probing 16 was used to monitor the transient yields of the CE ion signals to gain a greater understanding of the dynamical timescales involved in CE of the metastable PNT²⁺ and PNT³⁺ ions. Because the precursor ions cannot be detected directly in TOF-MS, we must rely on the transient signals of the CE product ions to infer the metastable lifetimes of PNT²⁺ and PNT³⁺ prior to CE. This strategy of inferring CE timescales of metastable precursors, using pump—probe measurements, to disrupt dissociation

processes yielding observed product ions has previously been employed to study the dynamics of CE pathways in the small molecules N₂O, CH₃OH, and CO₂, $^{2S-27}$ and the formation of H₃⁺ from dications of small alcohols.

To most efficiently disrupt the spontaneous CE of the metastable PNT²⁺ and PNT³⁺, it is necessary to choose a suitable probe wavelength that can electronically excite both metastable species. Computations of the excited electronic states of both PNT²⁺ and PNT³⁺ at the EOM-CCSD/cc-PVTZ level show that 400 nm (3.1 eV) photons can efficiently excite both PNT²⁺ and PNT³⁺ from their ground states (Figure 7).

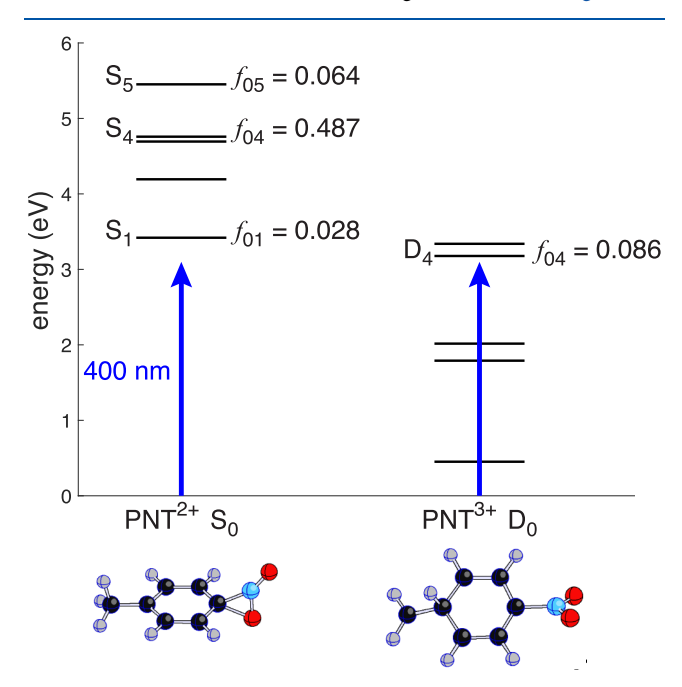


Figure 7. Energy levels of PNT²⁺ and PNT³⁺, calculated at the EOM-CCSD/cc-PVTZ level. Oscillator strengths for excited states with non-negligible coupling to the ground state are indicated. The energy of a 400 nm photon is shown for reference.

We assume that the probe pulse interacts with ground-state PNT²⁺ and PNT³⁺ because even if the pump pulse initially populated electronic excited states of these ions, relaxation to the ground electronic state most likely occurs on a shorter timescale than the 70 fs temporal resolution of the experiment. 46 The 400 nm probe provides nearly enough energy to excite PNT²⁺ in the S_0 state to S_1 , with a moderate oscillator strength $f_{01} = 0.028$. The 400 nm probe pulse is also nearly resonant with the $D_0 \rightarrow D_4$ transition in PNT³⁺ with moderately strong coupling of f_{04} = 0.086. We note that TDDFT computations of the low-lying PNT²⁺ and PNT³⁺ excited states at the ωB97X-D/aug-cc-PVTZ level produce excitation energies within 0.4 eV of the EOM-CCSD results and consistent assignments of bright states (Supporting Information, Tables S2-S4). Hence, we chose 400 nm for the probe wavelength in our experiments.

Pump—probe measurements were conducted using our previously reported setup²¹ with 1300 nm, 10^{14} W cm⁻² pump and 400 nm, 6×10^{12} W cm⁻² probe pulses. As expected, based on the predicted electronic structures of PNT²⁺ and PNT³⁺, the CE ion signals of NO₂⁺, $C_7H_7^+$, and $C_7H_2^{2+}$ are sensitive to the pump—probe delay, although the NO⁺ signal exhibits less change (Supporting Information, Figure S10). The transient ion signals as a function of pump—

probe delay au were fit using the method introduced by Jochim et al 16

$$S(\tau) = a e^{-\tau^2/s^2} + bP(\tau, T_d) + cP(\tau, T_r) + dP(\tau, T_{long}) + 1$$
(6)

where s=42.4 fs is obtained from the width of the cross-correlation function fwhm = $2\sqrt{\ln 2} s = 70.5$ fs. The first term in eq 6 simulates the instrument response function from the cross-correlation signal. The remaining terms $P(\tau, T_i)$ are given by

$$P(\tau, T_i) = \left[1 + \operatorname{erf}\left(\frac{\tau}{s} - \frac{s}{2T_i}\right)\right] e^{-\tau/T_i}$$
(7)

where each time constant T_i corresponds to a specific dynamical time scale. $T_{\rm d}$ defines a time constant associated with exponential decay of the signal, whereas $T_{\rm r}$ defines a time constant associated with exponential rise. The time constant $T_{\rm long}=10^5$ fs accounts for constant depletion or enhancement of the ion signal as $\tau\to\infty$, relative to its initial yield (i.e., at negative pump–probe delay). The coefficients a through d, along with $T_{\rm d}$ and $T_{\rm r}$, are determined by least squares curve fitting.

Figure 8 shows the transient CE ion signals of selected ions: (top panel) NO_2^+ assigned to initial PNT^{q+} charge states q=2 (red) and q=3 (green); (middle panel) $C_5H_2^+$ (orange) and CH_2^+ (cyan); and (bottom panel) $C_7H_7^+$ (magenta) and $C_7H_2^{2+}$ (blue). All signals are normalized to their yields at negative delay because the probe pulse produced no ions when the pump was blocked. The fit of each transient signal to eq 6 is shown as a solid line fit to the data points, along with the extracted time constants T_r and T_d (if present). All fit coefficients are given in Table 2. The mass spectral signals of these ions at selected pump—probe delays are given in the Supporting Information, Figures S10 and S11.

The time constant T_r is associated with the recovery of the ion signal near to its initial value after depletion at short positive delays. This transient depletion and recovery is due to the probe pulse disrupting the spontaneous dissociation of the multiply charged precursor ion. 16,22-26 Similarly, transient enhancement and decay with time constant $T_{\rm d}$ are associated with the initial enhancement of an ion signal due to excitation of the multiply charged precursor by the probe pulse, followed by decay due to depletion of the precursor population at longer delays. In this context, it is notable that the NO₂⁺ signal assigned to the q = 2 precursor has a substantially longer $T_r =$ 191 \pm 5 fs than NO₂ assigned to the q = 3 precursor with $T_r =$ 89 ± 5 fs. These distinct timescales suggest that the respective precursor ions have different lifetimes before CE, namely, PNT²⁺ survives for up to ~200 fs, whereas PNT³⁺ undergoes CE within less than 100 fs. Moreover, the dynamics of C₅H₂⁺ and CH_2^+ nearly mirror those of NO_2^+ assigned to q = 2 and q =3, respectively. The enhancement of C₅H₂⁺ and CH₂⁺ at short delays mirrors the depletion of both NO_2^+ signals, and the T_d = 260 \pm 20 fs for C₅H₂⁺ and $T_d = 100 \pm 20$ fs for CH₂⁺ roughly match the T_r values for the q = 2 and q = 3 signals from NO₂, respectively. Hence, we propose that excitation of the PNT2+ and PNT³⁺ by the probe pulse, prior to CE, forms C₅H₂⁺ and CH₂, respectively, although it is likely that additional fragments are also produced.

Further evidence for the ~200 fs lifetime of PNT²⁺ comes from $T_r = 240 \pm 70$ fs for its complementary ion $C_7H_7^+$, which

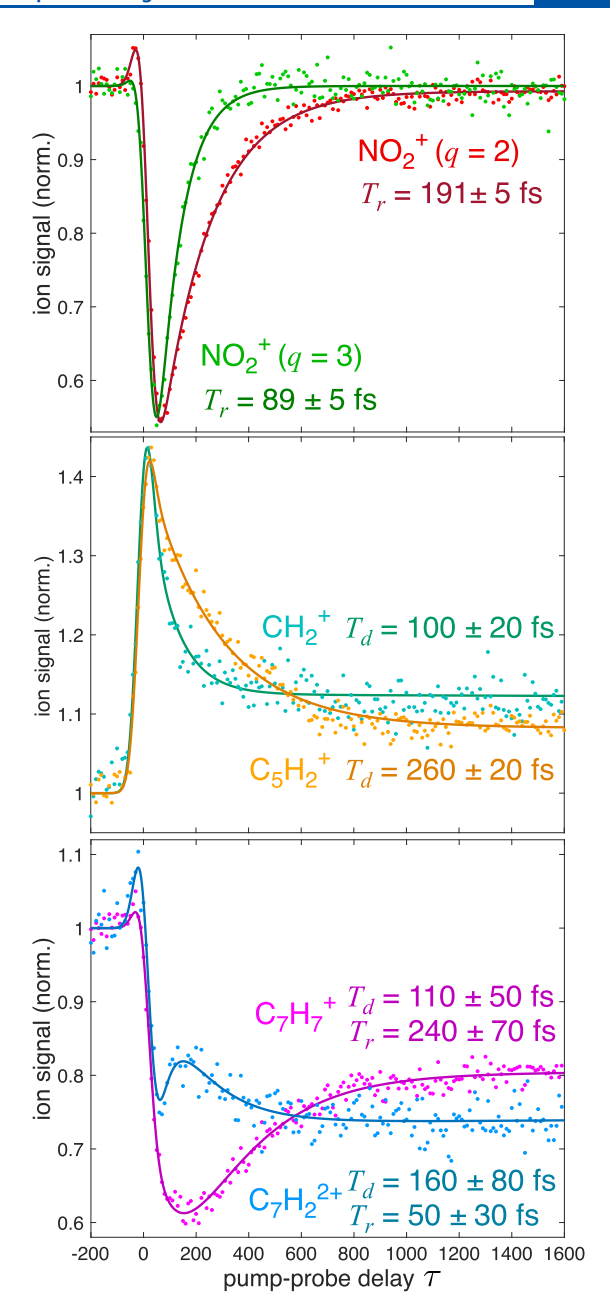


Figure 8. Transient ion signals (dots) of (top panel) NO₂⁺ assigned to q = 2 (red) and q = 3 (green); (middle panel) $C_5H_2^+$ (orange) and CH_2^+ (cyan); (bottom panel) $C_7H_7^+$ from CE (magenta) and $C_7H_2^{2+}$ (blue). Fits to eq 6 (solid lines) and extracted time constants T_d and T_r are indicated with errors denoting 95% confidence interval.

matches the T_r for NO_2^+ assigned to the q=2 precursor and the T_d for $C_5H_2^+$ to within the fitting error. We note that the presence of the additional $T_d=110\pm 50$ fs time constant is likely an artifact of the uncertainty in fitting the depleted $C_7H_7^+$ signal at short pump—probe delays because the CE peaks nearly disappear into the baseline noise (Supporting Information, Figure S10). Meanwhile, the substantially shorter $T_r=50\pm 30$ fs for $C_7H_2^{2+}$ is consistent with its formation from a shorter-lived precursor like PNT³⁺ or possibly PNT⁴⁺. Finally, the transient dynamics of the NO⁺ signals assigned to q=2 and q=3 precursors also support the conclusion that PNT²⁺ has a longer lifetime than PNT³⁺. We note that the extracted time constants for NO⁺ do not match those of NO⁺

Table 2. Coefficients Extracted from Fitting Transient Ion Signals in Figure 8 to Eq 6

signal	A	ь	$T_{\rm d}$ (fs)	с	$T_{\rm r}$ (fs)	d
$NO_2^+ (q = 2)$	0.24 ± 0.01			-0.34 ± 0.01	191 ± 5	-0.004 ± 0.001
$NO_2^+ (q = 3)$	0.18 ± 0.02			-0.48 ± 0.03	89 ± 5	
$C_5H_2^+$	0.16 ± 0.01	0.17 ± 0.01	260 ± 20			0.042 ± 0.002
CH_2^+	0.22 ± 0.03	0.15 ± 0.03	100 ± 20			0.062 ± 0.003
$C_7H_7^{+}$	0.11 ± 0.02	0.3 ± 0.2	110 ± 50	-0.3 ± 0.2	240 ± 70	-0.099 ± 0.003
$C_7 H_2^{2+}$	0.25 ± 0.05	0.2 ± 0.1	160 ± 80	-0.4 ± 0.1	50 ± 30	-0.133 ± 0.003

(Supporting Information, Figure S12). This discrepancy suggests that the rearrangement pathways proceed from different initial PNT²⁺ and PNT³⁺ electronic states, as compared to the direct pathways, which would be consistent with the weaker response of NO⁺ signals to the probe pulse (Supporting Information, Figures S10 and S12).

Unlike the transient NO₂ signals that recover to their initial yields once the CE is complete, both $C_7H_7^+$ and $C_7H_2^{2+}$ signals remain substantially depleted from their initial yields at long positive time delays. This permanent depletion suggests that the $C_7H_7^+$ and $C_7H_7^{2+}$ (a possible precursor to $C_7H_2^{2+}$) are themselves subjected to further excitation by the probe pulse after they are formed by CE. Indeed, previous spectroscopic and computational work on the benzylium $C_7H_7^+$ structure with $[C_6H_5-CH_2]^+$ topology indicates a moderately strong $S_0 \rightarrow S_1$ transition (f = 0.026) at around 410 nm, whereas the more stable tropylium 7-membered ring structure only absorbs wavelengths below 300 nm.47 To explore the hypothesis that $C_7H_7^+$ and $C_7H_7^{2+}$ can be further excited by the probe, their structures with the C₆H₄-CH₃ topology, which have higher energy than the lowest-energy isomers of each charge state by at least 2 eV (Supporting Information, Figure S13), were considered. The electronic excited states of these structures were computed at the ωB97X-D/aug-cc-PVTZ level using the TDDFT method (Supporting Information, Table S5). This level of theory is expected to adequately capture the low-lying excited states in both species on the basis of the qualitative agreement between TDDFT and EOM-CCSD results seen for PNT²⁺ and PNT³⁺ (Supporting Information, Tables S2–S4).

Figure 9 indicates low-lying excited states of both species with non-negligible coupling to the ground state, along with the 400 nm photon for reference. In $C_7H_7^+$, the 400 nm photon exceeds the energy of the weakly allowed $S_0 \rightarrow S_2$ transition ($f_{02} = 0.0005$), which can account for the modest ~15% depletion of $C_7H_7^+$ at long pump—probe delays. In $C_7H_7^{2+}$, the 400 nm photon can access the D_1 through D_3 states with weak coupling, which accounts for the extremely low yield of $C_7H_7^{2+}$, as seen in Figure 3b.

The ability of $C_7H_7^{2+}$ to absorb 400 nm photons can rationalize the complexity of the observed $C_7H_2^{2+}$ dynamics in Figure 8. The presence of fast T_r and slower T_d time constants indicates that $C_7H_2^{2+}$ results from sequential dissociation involving an intermediate, I, for example

$$PNT^{q+} \to I \to C_7 H_2^{2+} \tag{8}$$

The $C_7H_2^{2+}$ depletion at very early times (<100 fs) arises because the probe excites the PNT^{q+} to prevent the sequential reaction in eq 8. As the PNT^{q+} undergoes CE, the reduced efficiency of probe excitation leads to a rise in the $C_7H_2^{2+}$ signal, corresponding to $T_r = 50 \pm 30$ fs. At longer probe delays, the intermediate I absorbs 400 nm photons and further fragments into other species, resulting in a depleted $C_7H_2^{2+}$ signal with $T_d = 160 \pm 80$ fs. Although we cannot definitively assign the initial

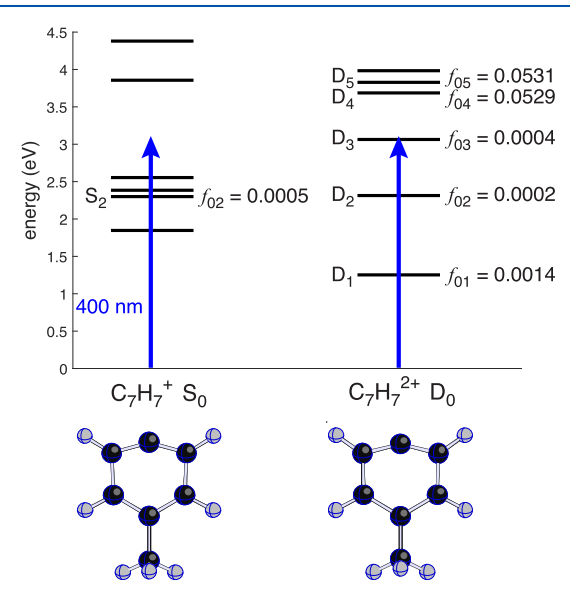


Figure 9. Energy levels of $C_7H_7^+$ and $C_7H_7^{2+}$, calculated at the ω B97X-D/aug-cc-PVTZ level. Oscillator strengths for excited states with nonnegligible coupling to the ground state are indicated. The energy of a 400 nm photon is shown for reference.

charge state PNT^{q+} or I in eq 8, the fact that $C_7H_7^{2+}$ can absorb 400 nm photons makes it a plausible species for I, and the short T_r makes PNT³⁺ a plausible initial state. However, we cannot rule out the possibility that $C_7H_2^{2+}$ is formed by a different pathway, from a more highly charged PNT^{q+} precursor. Finally, we note that the 400 nm photon cannot excite the linear $C_7H_2^{2+}$ species because computations of its excited states at the ω B97X-D/aug-cc-PVTZ level indicate no allowed transitions with energies lower than 5.5 eV (Supporting Information, Table S6).

3.4. Discussion. The combination of ultrafast disruptive probing measurements and theoretical computations in this work has revealed key new insights into the dissociation pathways and dynamics of multiply charged PNT cations, as summarized in Figure 10. In contrast to PNT+, which is stable unless excited to specific electronic excited states as discussed in our earlier work,²¹ both PNT²⁺ and PNT³⁺ are metastable with respect to NO₂ and NO⁺ loss (Figure 5) and have estimated lifetimes of \sim 200 fs for PNT²⁺ and \sim 90 fs for PNT³⁺ (Figure 8). Moreover, ionization to higher charge states PNT $^{q+}$, $q \ge 3$, produces a plethora of singly and multiply ionized dissociation products (Figures 2 and 3). Although these species and CE signatures in ion signals of NO₂ and NO⁺ have previously been observed in nitroaromatic molecules upon SFI, 10-14 neither pairs of CE ion signals in NO2 and NO⁺ associated with formation of PNT²⁺ and PNT³⁺ nor the timescales required for these CE processes have been reported previously.

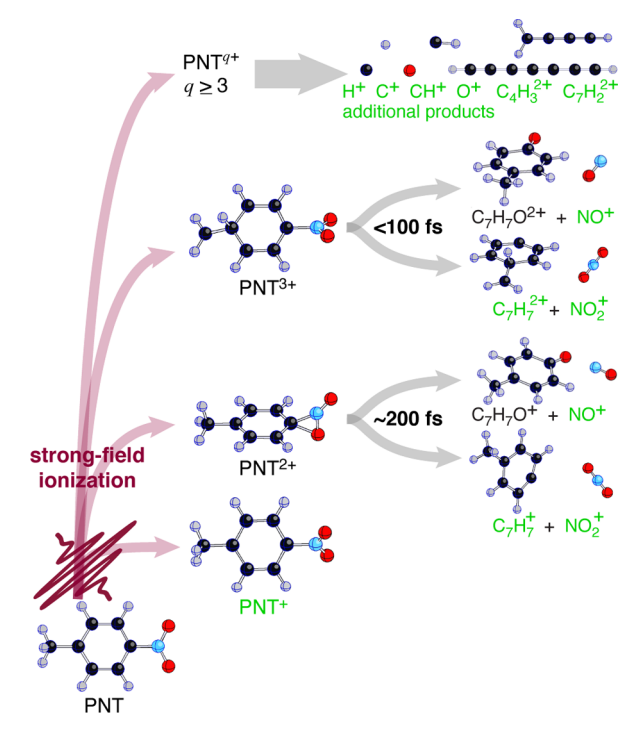


Figure 10. Summary of ionization and dissociation pathways in PNT induced by near-infrared strong field ionization. Dissociation timescales and products are indicated; products in green text are observed in mass spectra (Figure 3).

This application of ultrafast disruptive probing to determine CE timescales in PNT demonstrates the power of the technique for capturing dissociation dynamics of large multiply charged molecules beyond the small alcohols 22-25 and triatomic molecules^{26,27} studied previously. Although CE upon SFI of numerous complex molecules, including hexamethyldisilane, ⁴⁸ metal carbonyls, ⁴⁹ and 3,5-dibromo-3',5'-difluoro-4-cyanobiphenyl, ⁵⁰ have been reported, no dynamical timescales of CE or other dissociation pathways have been experimentally measured previously for any multiply charged cation larger than propanol.²³ Hence, this work suggests that ultrafast disruptive probing can provide a powerful complementary experimental technique for the ab initio molecular dynamics computations that are widely used to estimate dissociation timescales in dications of complex polyatomic molecules. $^{51-54}$ We note that future investigations of molecular dynamics simulations and ion-ion coincident imaging²² could further confirm the CE pathways and timescales reported here for PNT cations and clarify the origin of ions such as $C_7H_2^{2+}$; however, these studies are beyond the scope of the present work.

Finally, our results motivate further use of ultrafast disruptive probing to measure CE dynamics in energetic molecules. In particular, the clear resolution of the timescales required to produce NO₂⁺ from direct CE of PNT²⁺ and PNT³⁺ suggests that this technique could determine direct CE timescales in nitroaromatic explosives such as dinitrobenzene, dinitrotoluenes, and TNT, in which direct CE to produce NO₂⁺ has been observed upon SFI.¹³ Ultimately, this knowledge of ultrafast CE dynamics in energetic molecules can inform understanding of both shock and laser initiation mechanisms in energetic materials that involve transient formation of charged species.

4. CONCLUSIONS

This work explored CE dissociation pathways in multiply charged cations of PNT, a model compound for nitroaromatic energetic molecules like TNT. For the first time, we have observed experimental evidence of the metastable ions PNT²⁺ and PNT³⁺ that undergo CE to produce NO₂ and NO⁺. The experimentally measured released kinetic energies in NO2 of 4.1 ± 1.7 and 9.4 ± 2.7 eV from PNT²⁺ and PNT³⁺, respectively, agree with the computed energies of 3.26 and 6.72 eV to within experimental uncertainty. Similarly, the measured released kinetic energies in NO $^+$ of 4.6 \pm 2.4 and 9.6 \pm 5.0 eV from PNT²⁺ and PNT³⁺ agree within the error to the computed energies of 5.12 and 9.85 eV, respectively. Additional charged fragments identified by computed dissociation of highly charged PNT $^{q+}$ ions with q > 3 were observed in the mass spectra. We were further able to identify the dynamical timescales required for direct CE of PNT²⁺ and PNT³⁺, using ultrafast disruptive probing measurements, which identified timescales of ~200 and ~90 fs for direct CE of PNT²⁺ and PNT³⁺, respectively. These results indicate that ultrafast disruptive probing can be a useful technique for probing dissociation pathways in multiply charged cations in energetic materials and for other applications.

ASSOCIATED CONTENT

Supporting Information

The Supporting Information is available free of charge at https://pubs.acs.org/doi/10.1021/acs.jpca.2c04395.

Tabulated theoretical results of ionization, excited state energies, and oscillator strengths; additional figures of computed structures, magnified mass spectrometry data, and transient ion dynamics (PDF)

AUTHOR INFORMATION

Corresponding Author

Katharine Moore Tibbetts — Department of Chemistry, Virginia Commonwealth University, Richmond, Virginia 23284, United States; orcid.org/0000-0001-8853-5656; Email: kmtibbetts@vcu.edu

Authors

Jacob M. Shusterman – Department of Chemistry, Virginia Commonwealth University, Richmond, Virginia 23284, United States

Gennady L. Gutsev — Department of Physics, Florida A&M University, Tallahassee, Florida 32307, United States; orcid.org/0000-0001-7752-5567

Hugo A. López Peña – Department of Chemistry, Virginia Commonwealth University, Richmond, Virginia 23284, United States

B. Ramu Ramachandran — Institute for Micromanufacturing, Louisiana Tech University, Ruston, Louisiana 71272, United States

Complete contact information is available at: https://pubs.acs.org/10.1021/acs.jpca.2c04395

Notes

The authors declare no competing financial interest.

ACKNOWLEDGMENTS

Portions of this research were conducted with high-performance computational resources provided by the Louisiana

Optical Network Initiative (http://www.loni.org). G.L.G. and K.M.T. acknowledge the support of the U.S. Army Research Office through contract W911NF-19-1-0099. B.R.R. acknowledges the support from the National Science Foundation under Grant Number OIA-1946231. H.A.L.P. acknowledges the generous support of an Altria Graduate Research Fellowship.

REFERENCES

- (1) Reed, E. J.; Riad Manaa, M.; Fried, L. E.; Glaesemann, K. R.; Joannopoulos, J. D. A Transient Semimetallic Layer in Detonating Nitromethane. *Nat. Phys.* **2008**, *4*, 72–76.
- (2) Reed, E. J. Electron-Ion Coupling in Shocked Energetic Materials. J. Phys. Chem. C 2012, 116, 2205–2211.
- (3) Pellouchoud, L. A.; Reed, E. J. Optical Characterization of Chemistry in Shocked Nitromethane with Time-Dependent Density Functional Theory. *J. Phys. Chem. A* **2013**, *117*, 12288–12298.
- (4) Wang, B.; Wright, D.; Cliffel, D.; Haglund, R.; Pantelides, S. T. Ionization-Enhanced Decomposition of 2,4,6-Trinitrotoluene (TNT) Molecules. *J. Phys. Chem. A* **2011**, *115*, 8142–8146.
- (5) Furman, D.; Kosloff, R.; Dubnikova, F.; Zybin, S. V.; Goddard, W. A.; Rom, N.; Hirshberg, B.; Zeiri, Y. Decomposition of Condensed Phase Energetic Materials: Interplay between Uni- and Bimolecular Mechanisms. *J. Am. Chem. Soc.* **2014**, *136*, 4192–4200.
- (6) Bowden, M. D.; Cheeseman, M.; Knowles, S. L.; Drake, R. C. Laser Initiation of Energetic Materials: a Historical Overview. *Proc. SPIE* **2007**, *6662*, *6662*.
- (7) McGrane, S. D.; Bolme, C. A.; Greenfield, M. T.; Chavez, D. E.; Hanson, S. K.; Scharff, R. J. Photoactive High Explosives: Substituents Effects on Tetrazine Photochemistry and Photophysics. *J. Phys. Chem.* A **2016**, *120*, 895–902.
- (8) Herreros, D. N.; Fang, X. Laser Ignition of Elastomer-Modified Cast Double-Base (EMCDB) Propellant Using a Diode Laser. *Opt. Laser Technol.* **2017**, *89*, 21–26.
- (9) Ledingham, K. W. D.; Deas, R. M.; Marshall, A.; McCanny, T.; Singhal, R. P.; Kilic, H. S.; Kosmidis, C.; Langley, A. J.; Shaikh, W. A Comparison of Femtosecond and Nanosecond Multiphoton Ionization and Dissociation for Some Nitro-Molecules. *Rapid Commun. Mass Spectrom.* **1995**, *9*, 1522–1527.
- (10) Kosmidis, C.; Ledingham, K. W. D.; Kilic, H. S.; McCanny, T.; Singhal, R. P.; Langley, A. J.; Shaikh, W. On the Fragmentation of Nitrobenzene and Nitrotoluenes Induced by a Femtosecond Laser at 375 nm. *J. Phys. Chem. A* **1997**, *101*, 2264–2270.
- (11) Weickhardt, C.; Tönnies, K. Short Pulse Laser Mass Spectrometry of Nitrotoluenes: Ionization and Fragmentation Behavior. *Rapid Commun. Mass Spectrom.* **2002**, *16*, 442–446.
- (12) Tasker, A. D.; Robson, L.; Ledingham, K. W. D.; McCanny, T.; Hankin, S. M.; McKenna, P.; Kosmidis, C.; Jaroszynski, D. A.; Jones, D. R. A High Mass Resolution Study of the Interaction of Aromatic and Nitro-Aromatic Molecules with Intense Laser Fields. *J. Phys. Chem. A* 2002, 106, 4005–4013.
- (13) Mullen, C.; Coggiola, M. J.; Oser, H. Femtosecond Laser Photoionization Time-of-Flight Mass Spectrometry of Nitro-Aromatic Explosives and Explosives Related Compounds. *J. Am. Soc. Mass Spectrom.* **2009**, 20, 419–429.
- (14) Lozovoy, V. V.; Zhu, X.; Gunaratne, T. C.; Harris, D. A.; Shane, J. C.; Dantus, M. Control of Molecular Fragmentation Using Shaped Femtosecond Pulses. *J. Phys. Chem. A* **2008**, *112*, 3789–3812.
- (15) Gutsev, G. L.; McPherson, S. L.; López Peña, H. A.; Boateng, D. A.; Gutsev, L. G.; Ramachandran, B. R.; Tibbetts, K. M. Dissociation of Singly and Multiply Charged Nitromethane Cations: Femtosecond Laser Mass Spectrometry and Theoretical Modeling. *J. Phys. Chem. A* **2020**, *124*, 7427–7438.
- (16) Jochim, B.; DeJesus, L.; Dantus, M. Ultrafast Disruptive Probing: Simultaneously Keeping Track of Tens of Reaction Pathways. *Rev. Sci. Instrum.* **2022**, 93, 033003.
- (17) Word, M. D.; López Peña, H. A.; Ampadu Boateng, D.; McPherson, S. L.; Gutsev, G. L.; Gutsev, L. G.; Lao, K. U.; Tibbetts, K. M. Ultrafast Dynamics of Nitro-Nitrite Rearrangement and

- Dissociation in Nitromethane Cation. J. Phys. Chem. A 2022, 126, 879-888.
- (18) Ampadu Boateng, D.; Gutsev, G. L.; Jena, P.; Tibbetts, K. M. Dissociation Dynamics of 3- and 4-Nitrotoluene Radical Cations: Coherently Driven C-NO2 Bond Homolysis. *J. Chem. Phys.* **2018**, 148, 134305.
- (19) Ampadu Boateng, D.; Word, M. D.; Gutsev, L. G.; Jena, P.; Tibbetts, K. M. Conserved Vibrational Coherence in the Ultrafast Rearrangement of 2-Nitrotoluene Radical Cation. *J. Phys. Chem. A* **2019**, *123*, 1140–1152.
- (20) López Peña, H. A.; Ampadu Boateng, D.; McPherson, S. L.; Tibbetts, K. M. Using Computational Chemistry to Design Pump—Probe Schemes for Measuring Nitrobenzene Radical Cation Dynamics. *Phys. Chem. Chem. Phys.* **2021**, 23, 13338–13348.
- (21) López Peña, H. A.; Shusterman, J. M.; Ampadu Boateng, D.; Lao, K. U.; Tibbetts, K. M. Coherent Control of Molecular Dissociation by Selective Excitation of Nuclear Wave Packets. *Front. Chem.* **2022**, *10*, 859095.
- (22) Ekanayake, N.; et al. Mechanisms and Time-Resolved Dynamics for Trihydrogen Cation (H3+) Formation From Organic Molecules in Strong Laser Fields. *Sci. Rep.* **2017**, *7*, 4703.
- (23) Ekanayake, N.; et al. H2 Roaming Chemistry and the Formation of H3+ From Organic Molecules in Strong Laser Fields. *Nat. Commun.* **2018**, *9*, 5186.
- (24) Ekanayake, N.; Nairat, M.; Weingartz, N. P.; Michie, M. J.; Levine, B. G.; Dantus, M. Substituent Effects on H3+ Formation via H2 Roaming Mechanisms From Organic Molecules Under Strong-Field Photodissociation. *J. Chem. Phys.* **2018**, *149*, 244310.
- (25) Livshits, E.; Luzon, I.; Gope, K.; Baer, R.; Strasser, D. Time-Resolving the Ultrafast H2 Roaming Chemistry and H3+ Formation Using Extreme-Ultraviolet Pulses. *Commun. Chem.* **2020**, *3*, 49.
- (26) Gope, K.; Luzon, I.; Strasser, D. N-NO & NN-O Bond Cleavage Dynamics in Two- and Three-Body Coulomb Explosion of the N2O2+ Dication. *Phys. Chem. Chem. Phys.* **2019**, *21*, 13730–13737.
- (27) Bittner, D. M.; Gope, K.; Strasser, D. Time-Resolved Dissociative Ionization and Double Photoionization of CO2. *J. Chem. Phys.* **2020**, 153, 194201.
- (28) Lezius, M.; Blanchet, V.; Ivanov, M. Y.; Stolow, A. Polyatomic Molecules in Strong Laser Fields: Nonadiabatic Multielectron Dynamics. *J. Chem. Phys.* **2002**, *117*, 1575–1588.
- (29) Bohinski, T.; Moore Tibbetts, K. M.; Tarazkar, M.; Romanov, D.; Matsika, S.; Levis, R. J. Measurement of an Electronic Resonance in a Ground-State, Gas-Phase Acetophenone Cation via Strong-Field Mass Spectrometry. *J. Phys. Chem. Lett.* **2013**, *4*, 1587–1591.
- (30) Ampadu Boateng, D.; Gutsev, G. L.; Jena, P.; Tibbetts, K. M. Ultrafast Coherent Vibrational Dynamics in Dimethyl Methylphosphonate Radical Cation. *Phys. Chem. Chem. Phys.* **2018**, *20*, 4636–4640.
- (31) Tibbetts, K. M. Coherent Vibrational and Dissociation Dynamics of Polyatomic Radical Cations. *Chem.—Eur. J.* **2019**, 25, 8431–8439.
- (32) Chai, J.-D.; Head-Gordon, M. Long-Range Corrected Hybrid Density Functionals with Damped Atom-Atom Dispersion Corrections. *Phys. Chem. Chem. Phys.* **2008**, *10*, 6615–6620.
- (33) Dunning, T. H. Gaussian Basis Sets for Use in Correlated Molecular Calculations. I. The Atoms Boron Through Neon and Hydrogen. *J. Chem. Phys.* **1989**, *90*, 1007–1023.
- (34) NIST Standard Reference Database 69. http://webbook.nist.gov/chemistry/ (last checked June 01, 2022).
- (35) Krishnan, R.; Binkley, J. S.; Seeger, R.; Pople, J. A. Self-Consistent Molecular Orbital Methods. XX. A Basis Set for Correlated Wave Functions. *J. Chem. Phys.* **1980**, 72, 650–654.
- (36) Dreuw, A.; Head-Gordon, M. Single-Reference ab Initio Methods for the Calculation of Excited States of Large Molecules. *Chem. Rev.* **2005**, *105*, 4009–4037.
- (37) Stanton, J. F.; Bartlett, R. J. The Equation of Motion Coupled-Custer Method. A Systematic Biorthogonal Approach to Molecular Excitation Energies, Transition Probabilities, and Excited State Properties. *J. Chem. Phys.* **1993**, 98, 7029–7039.

- (38) Frisch, M.; Trucks, G.; Schlegel, H.; Scuseria, G.; Robb, M.; Cheeseman, J.; Scalmani, G.; Barone, V.; Mennucci, B.; Petersson, G.; et al. *Gaussian* 16, Rev. C.01; Gaussian, Inc.: Wallingford, CT, 2016.
- (39) Schlegel, H. Optimization of Equilibrium Geometries and Transition Structures. *J. Comp. Chem.* **1982**, *3*, 214–218.
- (40) Fukui, K. The Path of Chemical Reactions the IRC Approach. *Acc. Chem. Res.* **1981**, *14*, 363–368.
- (41) Hratchian, H.; Schlegel, H. Accurate Reaction Paths Using a Hessian Based Predictor-Corrector Integrator. *J. Chem. Phys.* **2004**, 120, 9918–9924.
- (42) Reed, A. E.; Curtiss, L. A.; Weinhold, F. Intermolecular Interactions From a Natural Bond Orbital, Donor-Acceptor Viewpoint. *Chem. Rev.* **1988**, *88*, 899–926.
- (43) Monfredini, T.; Fantuzzi, F.; Nascimento, M. A. C.; Wolff, W.; Boechat-Roberty, H. M. Single and Double Photoionization and Photodissociation of Toluene by Soft X-Rays in a Circumstellar Environment. *Atrophys. J.* **2016**, *821*, 4.
- (44) Nibarger, J. P.; Menon, S. V.; Gibson, G. N. Comprehensive Analysis of Strong-Field Ionization and Dissociation of Diatomic Nitrogen. *Phys. Rev. A: At., Mol., Opt. Phys.* **2001**, *63*, 053406.
- (45) Liu, H.; Yang, Z.; Gao, Z.; Tang, Z. Ionization and Dissociation of CH3I in Intense Laser Field. J. Chem. Phys. 2007, 126, 044316.
- (46) Adachi, S.; Kohguchi, H.; Suzuki, T. Unravelling the Electronic State of NO2 Product in Ultrafast Photodissociation of Nitromethane. *J. Phys. Chem. Lett.* **2018**, *9*, 270–273.
- (47) Dryza, V.; Chalyavi, N.; Sanelli, J. A.; Bieske, E. J. Electronic Absorptions of the Benzylium Cation. *J. Chem. Phys.* **2012**, *137*, 204304.
- (48) Yatsuhashi, T.; Nakashima, N. Dissociation and Multiply Charged Silicon Ejection in High Abundance from Hexamethyldisilane. *J. Phys. Chem. A* **2010**, *114*, 11890–11895.
- (49) Tanaka, H.; Nakashima, N.; Yatsuhashi, T. Anisotropic Coulomb Explosion of CO Ligands in Group 6 Metal Hexacarbonyls: Cr(CO)6, Mo(CO)6, W(CO)6. *J. Phys. Chem. A* **2016**, 120, 6917–6928.
- (50) Slater, C. S.; Blake, S.; Brouard, M.; Lauer, A.; Vallance, C.; Bohun, C. S.; Christensen, L.; Nielsen, J. H.; Johansson, M. P.; Stapelfeldt, H. Coulomb-Explosion Imaging Using a Pixel-Imaging Mass-Spectrometry Camera. *Phys. Rev. A: At., Mol., Opt. Phys.* **2015**, 91, 053424.
- (51) Maclot, S.; Piekarski, D. G.; Domaracka, A.; Méry, A.; Vizcaino, V.; Adoui, L.; Martín, F.; Alcamí, M.; Huber, B. A.; Rousseau, P.; Díaz-Tendero, S. Dynamics of Glycine Dications in the Gas Phase: Ultrafast Intramolecular Hydrogen Migration versus Coulomb Repulsion. *J. Phys. Chem. Lett.* **2013**, *4*, 3903–3909.
- (52) Piekarski, D. G.; Delaunay, R.; Maclot, S.; Adoui, L.; Martín, F.; Alcamí, M.; Huber, B. A.; Rousseau, P.; Domaracka, A.; Díaz-Tendero, S. Unusual Hydroxyl Migration in the Fragmentation of β-Alanine Dication in the Gas Phase. *Phys. Chem. Chem. Phys.* **2015**, *17*, 16767–16778.
- (53) Kukk, E.; Ha, D. T.; Wang, Y.; Piekarski, D. G.; Diaz-Tendero, S.; Kooser, K.; Itälä, E.; Levola, H.; Alcamí, M.; Rachlew, E.; Martín, F. Internal Energy Dependence in X-Ray-Induced Molecular Fragmentation: An Experimental and Theoretical Study of Thiophene. *Phys. Rev. A: At., Mol., Opt. Phys.* **2015**, *91*, 043417.
- (54) Wang, E.; Shan, X.; Chen, L.; Pfeifer, T.; Chen, X.; Ren, X.; Dorn, A. Ultrafast Proton Transfer Dynamics on the Repulsive Potential of the Ethanol Dication: Roaming-Mediated Isomerization versus Coulomb Explosion. *J. Phys. Chem. A* **2020**, *124*, 2785–2791.

☐ Recommended by ACS

What Determines the Drastic Reactivity of Nb_n+ Clusters with Nitric Oxide under Thermalized Conditions?

Benben Huang, Zhixun Luo, et al.

II II V 13 2022

THE JOURNAL OF PHYSICAL CHEMISTRY A

READ 🗹

Reaction of Ta_3 - Clusters with Molecular Nitrogen: A Mechanism Investigation

Xiaoli Sun and Xuri Huang

JUNE 21, 2022

ACS OMEGA

READ 🗹

NO Bond Cleavage on Gas-Phase Ir_n⁺ Clusters Investigated by Infrared Multiple Photon Dissociation Spectroscopy

Masato Yamaguchi, Fumitaka Mafuné, et al.

SEPTEMBER 20, 2022

THE JOURNAL OF PHYSICAL CHEMISTRY A

READ 🗹

Dinitrogen Activation by Dihydrogen and Quaternary Cluster Anions AuNbBO-: Nb- and B-Mediated N_2 Activation and Au-Assisted Nitrogen Transfer

Ying Li, Jia-Bi Ma, et al.

MAY 02, 2022

THE JOURNAL OF PHYSICAL CHEMISTRY LETTERS

READ 🗹

Get More Suggestions >